Eur. Phys. J. D **11**, 379–385 (2000)

THE EUROPEAN PHYSICAL JOURNAL D

EDP Sciences

Identification of structures in absorption spectrum of Kr–Xe gas mixtures close to the Xe resonance line at 146.96 nm

A. Morozov[1,a], B. Krylov[2], G. Gerasimov[2], R. Hallin[1], and A. Arnesen[1]

[1] Uppsala University, Department of Physics, Box 530, 75121 Uppsala, Sweden
[2] Vavilov state Optical Institute, Birzhevaja Line 12, St. Petersburg, 199034, Russia

Received 15 December 1999 and Received in final form 20 February 2000

Abstract. The origins of spectral structures that appear close to the Xe resonance line at 146.96 nm in absorption spectra of Kr gas with an admixture of Xe are discussed in this paper. It is shown that these structures can result from bound-bound and bound-free transitions in the Xe–Kr molecule between the ground state and the $1(^3P_1)$ excited state, which both are weakly-bound. The depth of the excited state is estimated. An introduction of a hump on the $1(^3P_1)$ state internuclear potential is suggested.

PACS. 33.20.Ni Vacuum ultraviolet spectra – 33.20.Tp Vibrational analysis

1 Introduction

Recently increasing attention has been paid to vacuum ultraviolet (VUV) emission spectra of heteronuclear rare gas diatomic molecules [1, 2]. This is connected with a number of practical applications such as broad band radiation sources [3, 4], and with discussions of the possibility to achieve VUV laser generation using heteronuclear rare gas molecules [5]. However, while the understanding of the internuclear potentials of the ground and excited states of homonuclear dimers is well established and seems to be quite reliable (see *e.g.* [6, 7]), the situation for heteronuclear dimers is less satisfactory. Detailed data exist only for the ground states [8], and were obtained by fitting theoretical potentials to a compilation of experimental results. Some information on the lowest excited states has been obtained by Castex [9] from absorption experiments and by Novak and Fricke [10] from surface VUV emission results. Theoretical investigations of the lowest excited states have been performed by Zagrebin and co-workers [11, 12], who obtained fundamental information on the internuclear potential curves for the lowest excited states. Application of these data in an attempt to define the origins of the observed spectral structures in emission and absorption could contribute to further adjustments of the shape and parameters of the internuclear potentials.

In this paper we discuss only the XeKr molecule. A basic scheme of internuclear potentials for the ground and the lowest excited XeKr molecular states (these excited states have their origins in the atomic Xe states $^3P_1$ and $^3P_2$) is presented in Figure 1. The potentials are shown in the Morse form. All excited-state potentials in Figure 1 are based on calculations [11], which predict the existence of bound (well depth about 1000 cm^{-1}) and weakly-bound (well depths about or less then 500 cm^{-1}) excited states.

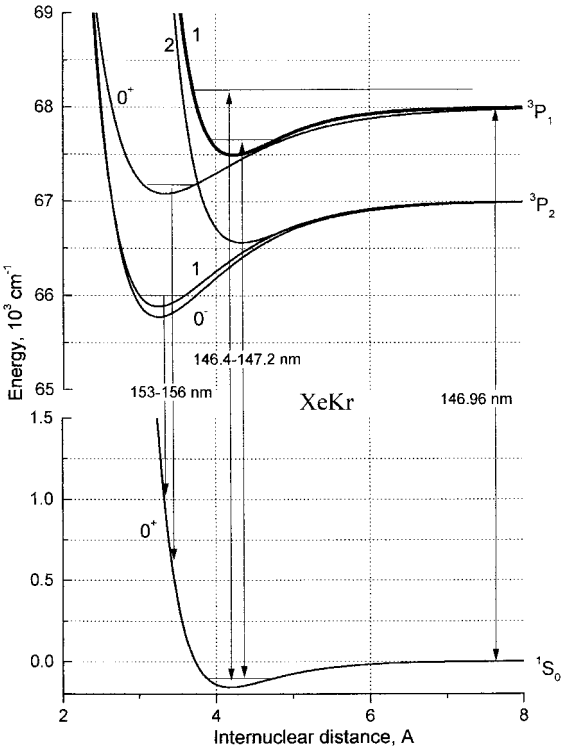

Fig. 1. Internuclear potentials for the ground and lowest excited states of the XeKr molecule. All curves are presented in the Morse form. Examples of bound and repulsive levels are shown by horizontal lines. Vertical arrows represent principal classes of transitions, including the atomic Xe^* resonance line and examples of bound-bound and bound-free transitions.

[a] e-mail: andreim@trym.fysik.uu.se

The weakly-bound states have equilibrium distances similar to that of the XeKr ground state, unlike the more strongly-bound excited states.

A Xe–Kr gas mixture emission spectrum shows a very intense and relatively narrow band around the Xe* resonance line at 146.96 nm (see [1]) with a width of 0.1–0.7 nm depending on the gas pressure. A reliable determination of the origins of this emission structure and detailed information on the internuclear potentials of the involved states would be useful for developing narrow band high intensity VUV radiation sources and for attempts to create a VUV laser working on molecular transitions in XeKr. In this article we present an attempt to analyse these potentials based on spectroscopic data.

We restrict our discussion to the state $1(^3P_1)$, since transitions from this state dominate the emission close to the Xe resonance line at 146.96 nm. This restriction is motivated by a number of facts: the atomic state $^3P_2$ is considerably shifted down in energy from the state $^3P_1$, so the transitions from the states $1(^3P_2)$ and $2(^3P_2)$ are situated at longer wavelengths; in addition the transition from the state $2(^3P_2)$ to the ground state is dipole forbidden. The relatively strongly-bound state $0^+(^3P_1)$ has an internuclear potential with a small equilibrium distance, so that emission from that state (similar in origin to the second continua of homonuclear dimers – see Fig. 1) appears as a broad continuum with maximum near 153 nm. Emission (absorption) from (to) this state close to 146.96 nm should also be small in comparison with emission (absorption) from (to) the state $1(^3P_1)$, because the weakly-bound state $1(^3P_1)$ has about the same potential well depth and equilibrium distance as the ground state, so the emission (absorption) from (to) this state will be more concentrated around the Xe* resonance line than for the $0^+(^3P_1)$ state. Moreover, due to the large difference in equilibrium distances between the ground and $0^+(^3P_1)$ states, their nuclear wave functions will have smaller overlap than the nuclear wave functions of the ground and $1(^3P_1)$ states.

However, it is quite difficult to identify the origins of the emission spectrum around 146.96 nm. No experimental emission data of high enough resolution (of the order of 0.001 nm) to be used as a detailed description of the bands have been published to our knowledge. Existing experiments show only general features, without the necessary details. Furthermore, for emission it is usually problematic to estimate relative populations of excited vibrational levels. In contrast to this, there are at least two high resolution experimental absorption studies performed by Castex [9] and Freeman *et al.* [13] (the resolution was 0.002 and 0.001 nm respectively) which describe absorption spectra around 146.96 nm in detail. Moreover, low resolution data (see *e.g.* our recently reported [1] results with a resolution of the order of 0.02 nm) show that emission and absorption spectra near the Xe resonance line at 146.96 nm exhibit remarkable similarity (Fig. 2), which indicates that corresponding spectral structures of both types of spectra have similar origins. The relative populations of the ground state vibrational levels are distributed according to Boltzmann statistics, and therefore easy to calculate. Furthermore, every emission spectrum around 146.96 nm from a Kr–Xe gas mixture light source is a combination of emission and self-absorption. This requires reliable and detailed information about the structure and origins of the absorption spectra in order to draw conclusions about the origins of the emission spectra. The discussion above indicates that elucidation of the origins of the emission spectral structures should be conducted after the origins of the absorption bands have been reliably established, which has not been done yet to our knowledge.

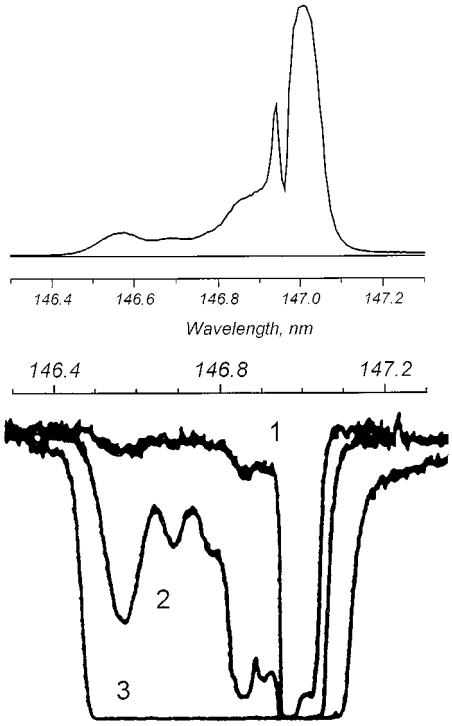

Fig. 2. An emission spectrum from a Kr–Xe gas mixture [1] (top spectrum) and absorption spectra recorded by Freeman *et al.* [13] (lower spectra) around the Xe I resonance line at 146.96 nm. The emission spectrum was obtained from a DC gas discharge (total gas pressure 120 hPa, Xe concentration 0.25%). Three absorption spectra are shown for the same Xe partial pressure 0.13 hPa and three different Kr pressures (1: 8 hPa, 2: 215 hPa, 3: 646 hPa).

In the next section we review the experimental absorption data to be used in the following discussion. These data will then be utilised to construct model internuclear potentials for the XeKr state $1(^3P_1)$ and to explain possible origins of the spectral structures. This will be done through qualitative analysis of the absorption spectra obtained by numerical simulations. These spectral simulations are obtained through calculations of the overlap of the nuclear wave functions of the ground state vibrational levels and bound or repulsive levels of the excited state (see Fig. 1). We do not expect the spectra obtained in this way to agree quantitatively with high resolution experimental spectra since model potentials have been used and rotational structure was beyond the scope of the present

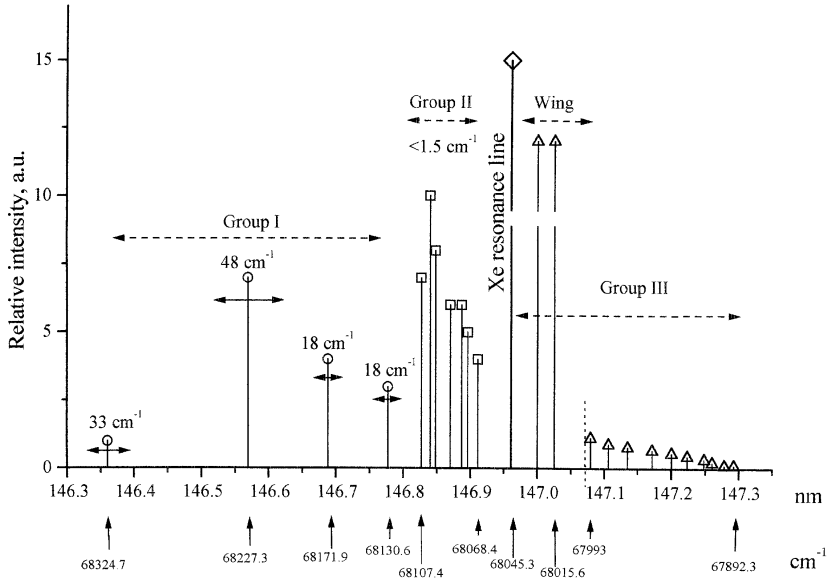

Fig. 3. A summary of experimental results obtained by Freeman *et al.* [13]. Vertical lines represent the positions (in nm and cm^{-1}) of spectral bands. Where it is available, the width of band is shown on top of the line. The Xe resonance line is marked with the diamond. Band group III (triangles) contains also the diffuse wing, adjoined to the resonance line: two of the most intense bands represent the maxima of the wing. Band group I (hollow dots) consists of four very broad and diffuse bands. Band group II (rectangles) is composed of seven very narrow bands with widths less than 1.5 cm^{-1}.

calculations. Our aim is, however, to be able to reproduce qualitatively all important spectral structures.

2 Review of available experimental data

According to Freeman *et al.* [13], three groups of discrete bands could be observed in the absorption spectra near the first resonance line of Xe I at 146.96 nm in Xe–Kr gas mixtures. In Figure 3 the results reported by Freeman in his Table I [13] are shown graphically: each observed band is represented by a vertical line at the appropriate wavelength, with the height proportional to the relative intensity of the band in its band group. The band's width is indicated if it was reported. The names of the absorption bands are the same as those used by Freeman [13].

As the first spectral feature, the broadened Xe I resonance line appears when only traces of Xe are added to Kr gas. On its long wavelength side the line has a wing containing three intensity maxima (146.961, 147.000 and 147.025 nm). At higher Xe concentration, more spectral features appear. The wing intensifies and broadens slightly towards long wavelengths but still exhibits a fairly sharp long wavelength edge. When $p(\mathrm{Xe}) \times p(\mathrm{Kr})$ reaches 0.4 torr^2 ($p(x)$ being the pressure of gas x), the sharp bands of band group II appear close to and on the short wavelength side of the resonance line (146.827–146.911 nm). All seven bands of this group have similar bandwidths of about or less then 1.5 cm^{-1} (0.003 nm). Here and onwards we use Freeman's pressure multiplication to show the relative intensities of band groups.

At slightly higher pressure, when $p(\mathrm{Xe}) \times p(\mathrm{Kr})$ is about 0.5 torr^2, the diffuse bands of band group I (146.360–146.777 nm, bandwidth from 18 to 46 cm^{-1}) appear on the short wavelength side of band group II. It was noted that band group I probably extends further towards longer wavelengths, but would be obscured by band group II.

Finally, at considerably higher pressure, when $p(\mathrm{Xe}) \times p(\mathrm{Kr})$ reaches 84 torr^2, with $p(\mathrm{Xe})$ at least 1.5 torr, band group III appears immediately to the long wavelength side of the fairly well-defined long wavelength edge of the broadened resonance line plus the wing. This group covers the range from 147.079 to 147.292 nm. No estimates were made of the bandwidth of the bands of that group.

In the Castex paper [9] only seven absorption bands were reported. The pressure and temperature dependencies of the blue satellite (Freeman's band groups I and II) and the red satellite (Freeman's wing) were discussed. The author reported that the blue satellite exhibits a strong temperature dependence, while the intensity of the red satellite changes only slightly with temperature. By analysing the pressure dependence the author drew the conclusion that Xe–Kr atomic pairs, bound or unbound, are responsible for the absorption around the Xe resonance line.

3 Computational technique

In the adiabatic approximation, the following formula is used to estimate the relative absorption probabilities W_{12} between a ground level 1 and an excited level 2 (bound or repulsive):

$$W_{12} \propto p_1 \left| \int \Psi_1(r) \mu_{12} \Psi_2(r) r^2 \mathrm{d}r \right|^2, \qquad (1)$$

where μ_{12} is the dipole transition moment, $\Psi(r) = P(r)/r$ are the radial parts of the nuclear wave functions for the ground and excited levels, and $P(r)$ are solutions of the radial Schrödinger equation:

$$\frac{\mathrm{d}^2 P}{\mathrm{d}r^2} + \frac{2m}{\hbar^2} \left[E - V(r) \right] P(r) = \frac{l(l+1)}{r^2} P(r). \qquad (2)$$

p_1 represents the relative population of a ground state vibrational level, which was calculated from the Boltzmann

distribution, and E is the energy – the eigenvalue for a bound level or the energy of a repulsive level.

In our calculations the dependence of the dipole transition moment on the internuclear distance is ignored, since no data on this dependence has been found in the literature. However, the dependence of the dipole transition moment on internuclear distance for heavy homonuclear inert dimers (see data on Ar_2, Kr_2 and Xe_2 in [14]) is relatively minor in comparison with the oscillations of the nuclear wave functions. It is therefore reasonable to conclude that in the case of heteronuclear dimers this simplification will not cause overly large deviations between the calculated and experimental spectra.

Nuclear wave functions for bound vibrational levels and for repulsive levels were calculated numerically. The code used to determine energy eigenvalues and nuclear wave functions is based on the method described by Hajj [15]. It is an iterative technique that determines the eigenvalue and produces the corresponding wave function by solving the Schrödinger radial equation (Numerov method). In the case of repulsive levels, the wave functions were normalised to a delta function in energy. The ground and excited state internuclear potentials were defined in numerical form or as mathematical functions.

We have tested the method on numerical calculations of eigenvalues for Morse potentials when these could also be determined analytically. A comparison of the results showed excellent agreement.

Results on simulations of absorption spectra for bound-bound and bound-free transitions are presented in this paper. For bound-bound transitions, the total absorption spectrum was obtained as the sum of the intensities of all possible transitions between vibrational levels of the excited and ground states with the weight factors $W_{12} = \exp\{-E/kT\}$ (see Eq. (1)), where E is the ground state vibrational level energy and T is the temperature. The spectrum is composed of a large number of transition lines, which makes it difficult to analyse it or compare it with experimental spectra. In experimental absorption spectra all these lines are broadened and superimposed due to limited resolution of the spectrometer and because of the presence of the rotational structure which "blurs" the spectrum. Therefore an additional simple recalculation of the absorption spectra was applied to imitate the limited resolution and rotational "blurring", the latter being beyond the scope of our calculations: the intensity $I(\lambda)$ at a succession of wavelengths λ in the range 146.0–147.4 nm, where each wavelength was separated from the next by a sufficiently small step to keep all spectral details, was calculated as the sum of all neighbouring transition line intensities I_i, multiplied by a Gaussian weight factor determined by the wavelength difference between the current wavelength λ and the transition line wavelength λ_i:

$$I(\lambda) = \sum_i I_i \exp\left[-\left(\frac{\lambda - \lambda_i}{\Delta/\sqrt{\ln 2}}\right)^2\right]. \qquad (3)$$

The HWHM of the Gaussian Δ was selected to be not less than the wavelength resolution of the experimental spectrum used as a model, and large enough to imitate rotational "blurring" of the spectrum.

For bound-free transitions, the total absorption spectrum is a sum of transition probability continua: each of them was obtained for a given ground vibrational level and a set of excited repulsive levels in the energy range from 5 to 400 cm^{-1} above the $^3P_1$ Xe^* atomic state with a step of 0.1 cm^{-1}. Each continuum also has a Boltzmann weight factor determined by the ground state vibration level energy.

4 Results and discussion

All calculations in this work were performed with the XeKr ground state taken in the Morse form:

$$V(r) = D\left[1 - \exp\{-\alpha(r - R_m)\}\right]^2 - D, \qquad (4)$$

where

$$\alpha = \frac{\ln(2)}{R_m - R_0}.$$

The following values of the parameters for the ground Morse potential were used: well depth $D = 159$ cm^{-1}, equilibrium distance $R_m = 4.18$ Å and zero-potential distance $R_0 = 3.73$ Å. The same values are used in the multiparameter potential of Lee [16]. By choosing these values for the simple Morse potential we obtain a quite good approximation for the more realistic, but very complex potential of Lee: the potentials are in very good agreement in their lower repulsive parts and around the equilibrium point. However, the Morse curve approaches the atomic origin faster than the potential of Lee, which gives 14 vibrational levels while the potential of Lee has 18 levels according to Bobetic and Barker [8]. We believe that the use of the Morse potential for the ground state is justified since we chose to use a Morse potential for the excited state.

The first spectral feature to identify is the most intense structure, namely the diffuse wing with several maxima located to the long wavelength side of the resonance line (Fig. 3). We have tried to demonstrate that this structure can be explained in the frame of bound-bound transitions between the ground state and the excited state $1(^3P_1)$ (Fig. 1). The result of our spectral simulation is presented in Figure 4. The excited state was taken in the Morse form with the following parameters: $D = 170$ cm^{-1}, $R_m = 4.4$ Å, $R_0 = 4.0$ Å. R_m and R_0 were taken directly from Zagrebin's calculations [11]. The value of $D = 500$ cm^{-1} given in [11] has lately been corrected to 300 cm^{-1} [17]. However, the proposed value of $D = 300$ cm^{-1} is too large according to our spectral simulations: the resulting spectral structure expanded much farther to the long wavelengths than in the experimental spectra. Therefore a more suitable value of 170 cm^{-1} was chosen and used instead. The position and width of the calculated structure as well as the location of the maximum are in rather good agreement with the experimental

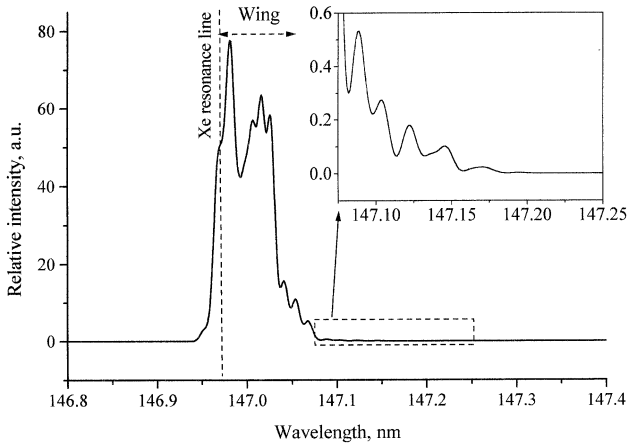

Fig. 4. Calculated absorption spectrum consisting of all possible transitions between bound vibrational levels of the ground state and the excited state $1(^3P_1)$. Both states have internuclear potentials in the Morse form. The inset shows the long wavelength spectral structure.

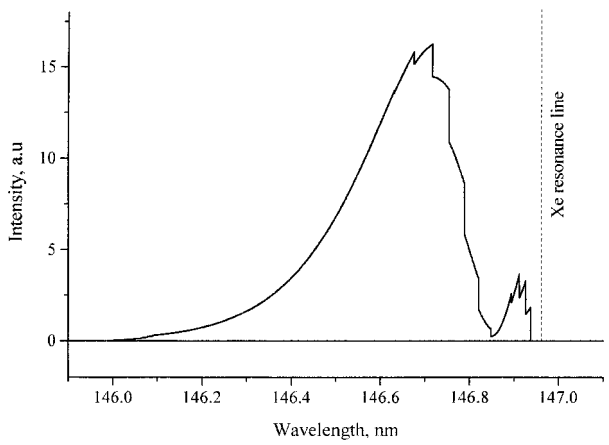

Fig. 5. Calculated absorption spectrum consisting of all possible transitions from ground state vibrational levels to the repulsive part of the excited state $1(^3P_1)$ from 5 cm^{-1} to 400 cm^{-1} above the $^3P_1$ Xe^* atomic state.

spectrum (compare the wing in Figs. 3 and 4). Of course, with the model potentials used and the assumptions that were made, one cannot expect detailed agreement. However, this calculations demonstrate that the wing can indeed have its origin in bound-bound transitions in XeKr molecules. This differs from the explanation that it is the broadened Xe atomic resonance line (transitions in free atomic pairs), which was proposed by Castex [9]. The temperature dependence of the wing, that was considered to be a proof of its atomic origin [9], will be discussed at the end of this section.

In Figure 4 an area directly adjoined to the long wavelength edge of the wing is expanded in a special window. One can see a number of peaks with much weaker intensities than the wing described above. We suggest that this structure (note that there is nothing similar on the short wavelength side of the resonance line) corresponds to the band group III (Fig. 3). It is quite possible that in a model using potentials which give a larger number of vibrational levels (*e.g.* the multiparameter potential of Lee [16]), this structure will intensify and expand slightly to longer wavelength. If this assignment of the origin of the band group III is correct, and this group does result from bound-bound transitions, the distance between the resonance line and the band with the longest wavelength gives the minimal depth of the excited state: 153 cm^{-1}. Observation of the emission spectrum around the resonance line [1] has shown that the relative intensity of the emission spectrum at the wavelengths of the band group III increases considerably with decreasing gas temperature. This could be explained by assuming that this band group originates from bound-bound transitions from the lowest excited vibrational levels, for which the relative populations increase considerably with gas cooling.

We now discuss the diffuse band group I. Within the framework of Morse-Morse potentials, the source of this group is very unlikely to be bound-bound transitions. Considering the band group I location, which is shifted significantly to shorter wavelength from the resonance line, and the large widths of the bands (see Fig. 3), the natural conclusion is that this group originates from bound-free transitions. In Figure 5, a calculated spectrum is shown. This spectrum is composed of the sum of all transitions from ground state vibrational levels to repulsive levels with energies given by the repulsive part of Morse potential of the state $1(^3P_1)$ (see Fig. 1). The following parameter values for the $1(^3P_1)$ state were used: $D = 170$ cm^{-1}, $R_m = 4.4$ Å and $R_0 = 3.7$ Å. The positions of maxima of the calculated structures and their widths are very sensitive to the Morse parameters of the excited state, especially on R_0. The spectrum shown in Figure 5 was obtained for the excited state with the same D and R_m as in our discussion of the wing (band group III) and only R_0 has been adjusted to achieve a total width of the structure close to the width observed in the experiments. Note that the "teeth" on the spectral profile are due to the fact that the total spectrum is a sum of partially overlapping continua where every "tooth" is in the place where the next continuum starts. Each continuum was obtained for transitions from a certain ground state vibrational level to an unbound level of the excited state with energy ranging from 5 to 400 cm^{-1} counted from the $^3P_1$ Xe^* atomic level. This range was taken because no spectral structures have been seen further than 400 cm^{-1} towards shorter wavelengths. Furthermore, energies less then 5 cm^{-1} give wave functions with very slow oscillations, which result in calculational difficulties, but do not provide much additional information. To summarise the results on band group I, we believe that the position and width of band group III as well as the number and widths of its maxima can be simulated through bound-free transition between potentials mentioned above (only small changes of the parameter values are required). However, the numerical fitting to experimental spectra would require considerable effort, which makes no sense until reliable and detailed data are obtained for one of the potentials (the ground or excited

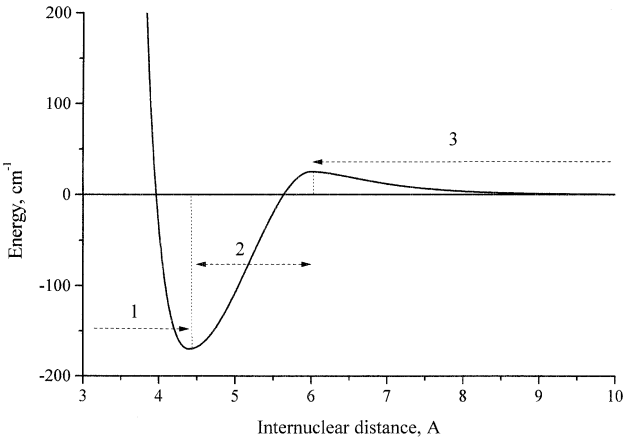

Fig. 6. The $1(^3P_1)$ state internuclear potential, containing a hump. The potential is composed of three parts: part 1: ordinary Morse potential for internuclear distances from 0 to equilibrium distance. Part 2: third degree polynomial. Part 3: Morse potential with negative sign from the hump maximum (corresponds to the equilibrium distance) and towards infinity.

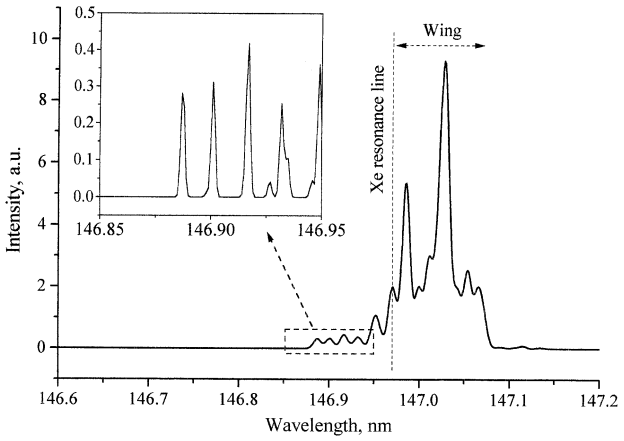

Fig. 7. Calculated absorption spectrum consisting of all possible transitions between vibrational levels of the ground state and the state $1(^3P_1)$ containing the hump. The inset shows the short wavelength spectral structure composed of relatively intense and narrow lines.

state) and for the dependence of the dipole transition moment on the internuclear distance.

We find the identification of the band group II to be the most problematic. It consists of seven sharp and intense bands, especially in comparison with the weak band group III. We believe that such narrow bands could not be observed in bound-free transitions between two Morse potentials: the slope of the repulsive part is too sharp, which will result in broad structures in the spectra. On the other hand, the bands are too intense to be assigned to bound-bound transitions between two Morse potentials, which still could explain the wing (compare Figs. 3 and 4). The problem could be solved by a considerable change of the shape of the excited state internuclear potential. Two different cases are discussed in the following paragraphs.

I. The band group II is assumed to originate in bound-free transitions with a non-Morse excited state. We have found that transitions between the ground Morse potential and a purely repulsive excited potential could result in sufficiently sharp bands. However, for the excited Xe* atomic state $^3P_1$ there are only two possible XeKr states: 0^+ and 1. The state $0^+(^3P_1)$ is bound (emission from this state appears with a broad maximum around 153 nm), and the state $1(^3P_1)$ has to be weakly bound (as discussed above) to explain the wing and the band groups III. There is, however, a compromise: the weakly-bound state $1(^3P_1)$ potential could have a "hump" (see Fig. 6). This potential has both a bound part at small internuclear distances and a slightly sloping repulsive part after the hump at large distances. We have constructed a model potential of that type in the following way: the potential consists of a Morse curve for small internuclear distances up to the equilibrium distance ($D = 170$ cm^{-1}, $R_m = 4.4$ Å, $R_0 = 4.0$ Å), then a 3rd degree polynomial until the hump maximum is reached and then a long-distance tail of another Morse potential taken with negative sign ($D = -25$ cm^{-1}, $R_m = 6.5$ Å, $R_0 = 6.0$ Å). This potential was numerically tested and it was found that the bound-free transitions from the ground state vibrational levels $\nu = 7$ and 8 give very narrow bands with FWHM less then 1.5 cm^{-1} as the band group II has. Bands from levels $\nu = 6$ and 9 gave narrow peaks with low intensity broad shoulders. The rest of the vibrational levels gave relatively low intensity broad structures. This demonstrates the possibility that all 7 observed bands could have the same origin (after a slight modification of the excited state potential) in bound-free transitions from the ground state to an excited state with a hump.

One should note that it is possible to apply the same considerations if we assume that the band group II originates from bound-free transitions between the weakly bound ground state and the excited state $0^+(^3P_1)$ if we introduce the same hump as for the $1(^3P_1)$ state.

II. The band group II could also result from bound-bound transitions in the case of a non-Morse excited state. An absorption spectrum corresponding to transitions between vibrational levels in the bound parts of the ground potential and the humped excited state potential described above is shown in Figure 7. There are sufficiently intense bands at the wavelengths of band group II, and still, as for Morse potentials, there are the wing and the weak structure where band group III is situated. However, the question of the width of the bands is still open: how could bands situated far from the centre of the wing (wavelength of band group II) be narrow while the centre of the wing is totally diffuse (according to Freeman *et al.* [13]). The answer might be given if also the rotational structure is taken into account, but this is beyond the model used in this work.

Analysis of rotational structure should also help to determine which alternative gives rise to, or dominates, the experimental spectra, that is whether the band group I originates from bound-bound or bound-free transitions.

One should note that the introduction of the hump for the $1(^3P_1)$ state to explain the band group II will not

lead to drastic changes in the remaining spectral ranges. This is connected with the fact that the humped potential described above has the same depth and equilibrium distance as the Morse potential used to calculate the bound-repulsive spectrum between two Morse potentials. Moreover, we inherited the repulsive part of the "humped" potential directly from the Morse potential. The result is that the bound-bound spectrum between the humped excited state and the ground state taken in the Morse form (see Fig. 7) still shows the diffuse wing with the right width and the low-intensity structure at the wavelength of the band group III. The shape of the wing will be different but as we pointed out, we do not expect detailed agreement. The diffuse structure at the place of the band group I will not change drastically either – the further from the resonance line the more similar the structure becomes to the one presented in the Figure 5.

Finally we consider the temperature dependence of the intensity of long and short wavelength structures around the resonance line in the absorption spectra. Castex [9] reported that the short wavelength satellite (corresponding to Freeman's band groups I and II) has a strong temperature dependence – its intensity increases with cooling of the absorbing gas, while the intensity of the long wavelength wing depends only slightly on the gas temperature. The explanation [9] was that the long wavelength satellite, corresponding to Freeman's wing, is due to transitions in free pairs (atomic line broadening), which has a very weak temperature dependence in comparison with bound-free transitions which give the short wavelength satellite. However, another explanation of the temperature dependence can be given by assuming a bound-bound origin of the long wavelength satellite. The intense part of the long wavelength satellite is composed mainly of all transitions with small differences in vibrational quantum number ν between the ground and excited state vibrational levels ($\nu = 0, \pm 1$ are dominating). This means that all, low as well as high, ground state vibrational levels contribute to the satellite. Decreasing the temperature and thereby increasing the relative population of lower vibrational levels in accordance with the Boltzmann factor, we only change the shape of the satellite, increasing some and decreasing other closely situated components without a considerable change of the total intensity. On the other hand, the dominant part of the short wavelength satellite, which is situated far from the resonance line, receives its main contribution from transitions starting from vibrational levels close to the bottom of the ground state potential well. For example, a change of temperature from 300 K to 165 K will result in an increase of the relative population of the vibrational level $\nu = 0$ with respect to the level $\nu = 14$ from 2:1 to 4:1, which causes a considerable growth of the absorption intensity in this structure.

5 Conclusion

We have demonstrated by numerical simulation that all spectral structure in the absorption spectrum around the Xe resonance line at 146.96 nm in Kr gas with an admixture of Xe can be explained by bound-bound and bound-free transitions between the ground XeKr state and the weakly-bound excited state $1(^3P_1)$. This explanation is supported by the dependence of the absorption and emission spectra on gas temperature. The depth of the potential well for the excited state $1(^3P_1)$ is estimated to be 170 cm^{-1}. To explain the part of the short wavelength structure that contains a number of narrow bands, we suggest the following modification of the excited state $1(^3P_1)$ potential: the weakly-bound state potential may have a hump with a maximum height of about 25 cm^{-1} at an internuclear distance near 6 Å.

We thank Professor A. Devdariani from St. Petersburg University and Professor L. Karlsson from Uppsala University for very useful advice and discussions. We are grateful to Dr. Zagrebin from St. Petersburg University for sending the results of his latest calculations. This project has been supported by the Swedish Research Council for Engineering Sciences (TFR) and Uppsala University.

References

1. B. Krylov, G. Gerasimov, A. Morozov, A. Arnesen, R. Hallin, F. Heijkenskjold, Eur. Phys. J. D **8**, 227 (2000).
2. T. Efthimiopoulos, D. Zouridis, A. Ulrich, J. Phys. D: Appl. Phys. **30**, 1746 (1997).
3. S. Kubodera, M. Kitahara, J. Kawanaka, W. Sasaki, K. Kurosawa, Appl. Phys. Lett. **69**, 452 (1996).
4. J. Wieser, D.E. Murnick, A. Ulrich, H.A. Huggins, A. Liddle, W.L. Brown, Rev. Sci. Instrum. **68**, 1360 (1997).
5. P.J.M. Peters, H.M.J. Bastiaens, in *Gas Lasers – Recent Developments and Future Prospects*, edited by W.J. Witteman, V.N. Ochkin (Kluwer Academic Publishers, 1996).
6. J.A. Barker, R.O. Watts, J.K. Lee, T.P. Schafer, Y.T. Lee, J. Chem. Phys. **61**, 3081 (1974).
7. W.C. Ermler, Y.S. Lee, K.S. Pitzer, N.W. Winter, J. Chem. Phys. **69**, 976 (1978).
8. M.V. Bobetic, J.A. Barker, J. Chem. Phys. **64**, 2367 (1976).
9. M.C. Castex, J. Chem. Phys. **66**, 3854 (1977).
10. G. Novak, J. Fricke, J. Phys. B: At. Mol. Phys. **18**, 1355 (1985).
11. A.L. Zagrebin, N.A. Pavlovskaya, Opt. Spectrosc. (USSR) **69**, 320 (1990).
12. A.Z. Devdariani, A.L. Zagrebin, K.B. Blagoev, Ann. Phys. Fr. **14**, 467 (1989).
13. D. Freeman, K. Yoshino, Y. Tanaka, J. Chem. Phys. **67**, 3462 (1977).
14. A.A. Madej, B.P. Stoicheff, Phys. Rev. A **38**, 3456 (1988).
15. F.Y. Hajj, J. Phys. B: At. Mol. Phys. **13**, 4521 (1980).
16. J.K. Lee, D. Henderson, J.A. Barker, Mol. Phys. **29**, 429 (1975).
17. A.L. Zagrebin, private communications.